Pergamon

Int. J. Heat Mass Transfer. Vol. 38, No. 2, pp. 317–329, 1995

0017–9310/95 $9.50+0.00

0017–9310(94)00150–2

Experimental analysis of intermaterial surfaces in the study of gaseous mixing characteristics

A. CAVALIERE and M. EL-NAGGAR

Dipartimento di Ingegneria Chimica, Università degli Studi di Napoli Federico II, P.zza Tecchio 80, 80125—Napoli, Italy

and

R. RAGUCCI

Istituto di Ricerche sulla Combustione, C.N.R., P.zza Tecchio 80, 80125—Napoli, Italy

(*Received* 10 *December* 1993 *and in final form* 18 *April* 1994)

Abstract—A unique experimental method for analysing mass transfer between gaseous flows has been presented. It consists of the measurement of Lagrangian quantities, linked to intermaterial surfaces evolution generated by means of a pulsed smoke wire technique. Stretch intensity, stretch rate, mixing-layer thickness, separation distance between neighbouring segments of the interface, for a purposely designed prototypical quasi-two-dimensional flow configuration, have been measured against time and presented in terms of their statistical distribution and averages. A peculiar regime named 'isolated mixing-layer regime' has been identified by means of comparison of the mixing-layer thickness with the interface separation distance. Further, the direct experimental evaluation of the stretch rate of the intermaterial surface allows the evaluation of the role of the kinematics on reactive mixing-layers, in particular in the case of the stretched diffusion flame.

1. INTRODUCTION

A great part of flow characterizations is based on Eulerian measurements, in the sense that the measurements are performed in fixed positions with respect to fixed coordinate systems. For instance the characterizations of turbulent flows are mainly obtained by means of single or multi-point temporal correlations and therefore they are inferred only on 'local' or 'quasi-local' characteristics of the turbulence.

It is known that some classes of flows are better evaluated by means of Lagrangian quantities. These flows are mainly related to mixing, since in this case the molecular diffusion can be considered in a much simpler way when it is linked to Lagrangian evaluation of some peculiar characteristics like the 'stretching' and 'folding' of single [1, 2] or multiple [3] material surfaces. This is of particular interest in the analysis of mixing reactive layers [4–8] because, only in this case, a detailed chemical kinetics description can be considered feasible in the numerical modelling of the process. These statements will be more clearly analysed in the part of this paper devoted to the discussion, using some preliminary definitions that will be given in the following section.

The main difficulty with the measurement of Lagrangian quantities, which are the basis of the aforementioned descriptions, is due to the fact that the quantities have to be detected in a three-dimensional domain which is not known *a priori* and can change in a time-dependent process as in a turbulent one. A much larger number of detectors (corresponding to different spatial points) have to be active in respect to those used during a single Lagrangian measurement.

This difficulty is even greater when the quantity is tensorial and multidimensional. In fact, in the case of tensorial quantities, multiple detectors have to be used for each single component of the tensor. For instance, the three components of the velocity have to be measured separately. Also, in the case of multidimensional quantities, multiple detectors have to be used with the additional difficulty that they have to be contiguous. For instance, the measure of a surface area which is placed in a three-dimensional (3-D) domain requires an ensemble of detectors which cover the whole domain.

Finally, a further complexity is related to possible different requirements of spatial and temporal resolutions in determining contemporaneously both the quantity and its evolution. For instance the temporal growth rate of a surface area with linear extension of 10^{-3} m can hardly be followed if the surface is displaced for a distance greater than 1 m, because measurements from an object field with extension of 1 m have to be collected with a spatial resolution of 10^{-4} m, if a 10% accuracy is needed when determining the line extension. This means, in a one-dimensional (1-D) domain, a detector with 10^4 elements is needed, and in a two-dimensional (2-D) domain, 10^8 elements. Due to these difficulties, Lagrangian measurements

NOMENCLATURE

a	intermaterial surface area
A	initial intermaterial surface area
A_w	smoke wire cross-section
d_p	particle diameter
D	mass diffusivity
E_w	electric energy supplied to the smoke wire
erf	error function
K	stretch rate
l_w	smoke wire length
$\mathbf{n}$	normal unit vector to the intermaterial surface
$\mathbf{r}$	position vector
R_w	electric resistance of smoke wire
Sc	Schmidt number
SR	stretch ratio
St	Stokes number
t	time
t^*	characteristic time
V_w	electric voltage supplied to the wire
Y	mass fraction
Z	distance normal to the intermaterial surface.

Greek symbols

δ, $\delta_{0.9}$	mixing-layer thickness
Δn	interface separation distance
Δt	time interval between two consecutive detected material surfaces
Δt_w	width of the electric pulse applied to the smoke wire
ΔV	velocity differences across the mixing layer
μ	dynamic viscosity
ν	kinematic viscosity
ρ	density
ρ_w	resistivity of the wire
τ	aerodynamic time-scale.

Subscripts

g	gas
p	particles
o	initial condition
α	passive scalar.

have rarely been used for detailed experimental description of fluid-dynamic controlled processes.

This paper faces such problems and presents some Lagrangian types of measurement which could be performed, because some of the previous difficulties have been avoided by contrivances regarding both the experimental diagnostics and the flow. In particular, the choice of using a quasi-2-D experimental configuration simplified the detection of Lagrangian measurements because the spatial domain in which the quantity can evolve is much narrower compared to the 3-D configuration and the available detectors can be exploited in more convenient ways so that space-resolved measurements can be performed.

2. SURFACE PROPERTIES

2.1. *Stretch ratio and stretch rate*

Definitions of surface properties are given in this section for reference in the following parts of the paper. The basic definition, by which all the other ones are derived is the 'area stretch ratio', which has been named by other authors as simply 'area stretch' [1, 2] or 'area amplification factor' [6]. This is a quantity [1] that refers to an initial infinitesimal surface located in a space point $\mathbf{r}_o$ at time t_o of initial area dA and orientation $\mathbf{n}_o$ (normal to the surface in $\mathbf{r}_o$, t_o). This initial infinitesimal surface evolves in time yielding an infinitesimal surface of area da and orientation $\mathbf{n}$. The stretch ratio SR is given by:

$$SR(t)|_{\mathbf{r}_o, t_o, \mathbf{n}_o} = \lim_{dA \to 0} \frac{da}{dA}. \tag{1}$$

It is of interest, for what will be presented in the following, to define a quantity named 'finite' stretch ratio $\widetilde{SR}$ given by:

$$\widetilde{SR}(t)|_{S(\mathbf{r}, t_o) = 0} = \frac{\Delta A(t)}{\Delta A(t_o)}. \tag{2}$$

In this case the ratio is between two finite area values (at time t_o and t) referred to a surface element, which evolves according to a law symbolically given by $S(\mathbf{r}, t) = 0$. The case $S(\mathbf{r}, t) = 0$ can be approximated by a planar surface with a known centre; the surface can be [analogously to equation (1)] specified in terms of R_o and $\mathbf{n}_o$.

The rate of stretch change is usually named stretch rate K or, by some authors [2, 9] 'stretching function'. This quantity is given by logarithmic time derivative of the stretch ratio and it is known as the finite stretch rate ($\tilde{K}$) when it refers to $\widetilde{SR}$:

$$K(t)|_{\mathbf{r}_o, t_o, \mathbf{n}_o} = \frac{D \ln SR}{Dt}, \tag{3}$$

$$\tilde{K}(t)|_{S(\mathbf{r}, t_o) = 0} = \frac{D \ln \widetilde{SR}}{Dt}. \tag{4}$$

The temporal averages of the stretch rate ($\bar{K}$ and $\bar{\tilde{K}}$) on a time interval Δt will be given by the following equations:

$$\bar{K}(t)|_{\mathbf{r}_o, t_o, \mathbf{n}_o, \Delta t} = \frac{1}{\Delta t}\int_{t-(\Delta t/2)}^{t+(\Delta t/2)} K \mathrm{D}t, \tag{5}$$

$$\bar{\tilde{K}}(t)|_{S(\mathbf{r}, t_o)=0, \Delta t} = \frac{1}{\Delta t}\int_{t-(\Delta t/2)}^{t+(\Delta t/2)} \tilde{K} \mathrm{D}t. \tag{6}$$

Equation (6) can also be expressed in terms of $\widetilde{SR}$, since $\tilde{K}$ can be written as:

$$\bar{\tilde{K}}(t) = \frac{1}{\Delta t}\int_{t-(\Delta t/2)}^{t+(\Delta t/2)} \frac{\mathrm{D}\ln \widetilde{SR}}{\mathrm{D}t}\mathrm{D}t$$

$$= \frac{1}{\Delta t}\ln\left[\frac{\widetilde{SR}\left(t+\frac{\Delta t}{2}\right)}{\widetilde{SR}\left(t-\frac{\Delta t}{2}\right)}\right]. \tag{7}$$

2.2. *Material and intermaterial surface*

In the definition given above, we have not explicitly mentioned the concept of the material surface, because the stretch ratio and stretch rates can also be of interest to different types of surfaces, for instance flame surfaces, but they have been referred implicitly to material surfaces because we have used the material derivative symbols in defining the stretch rates.

In the following, we will refer always to surface elements which are 'material' so that it is worthwhile explicitly defining this concept.

A material surface is defined as a surface element (arbitrarily defined at time t_o) constituted by points which are purely convected by the flow or, in other words, which move with the average mass velocity [1].

In a mixing process, a peculiar material surface is of interest. It is named the intermaterial surface [1], that is a material surface which is chosen on an interface. By 'interface' we mean a hypothetical surface on which the concentration gradient of a tracer (present only in the part of the flow which has to be mixed) becomes infinite. Finally, by a tracer we mean a hypothetical material which is purely convected according to the material derivative of its mass fraction Y_T:

$$\frac{\mathrm{D}Y_T}{\mathrm{D}t} = 0.$$

2.3. *Mixing layer*

We consider the mass balance of a conserved passive scalar α in terms of its mass fraction Y_α with respect to a coordinate system attached with its origin to the centre of an intermaterial surface and with the z-axis oriented in the direction of the normal to the intermaterial surface. Under the hypotheses fully discussed by previous authors [1, 2, 6], concerning the fact that mass fraction gradients along the axes parallel to the intermaterial surface are negligible with respect to gradient components along z, the mass balance can be given by:

$$\frac{\partial Y_\alpha}{\partial t} - Kz\frac{\partial Y_\alpha}{\partial z} - D\frac{\partial^2 Y_\alpha}{\partial z^2} = 0, \tag{8}$$

where D is the mass diffusivity of the species α in the mixture and K is the stretch rate defined by means of equation (3).

Equation (8) under the following transformation:

$$\zeta = z \cdot SR, \quad \tau = \int_o^\infty SR^2(t)\,\mathrm{d}t \tag{9}$$

can be written into the following equivalent form [1, 10]:

$$\frac{\partial Y_\alpha}{\partial \tau} - D\frac{\partial^2 Y_\alpha}{\partial \zeta^2} = 0. \tag{10}$$

Equation (10) is solved by a combination of variable transformation which yields a solution of Y_α, based on the error function (*erf*) of the non-dimensional variable $(z/\delta_{0.9})$ [11]:

$$\frac{Y_\alpha - Y_{\alpha_o}}{Y_{\alpha_\infty} - Y_{\alpha_o}} = erf(z/\delta_{0.9}), \tag{11}$$

where $\delta_{0.9}$ is the mixing-layer thickness defined as the distance from the coordinate origin of the point where:

$$\frac{Y_\alpha(z=\delta_{0.9}) - Y_\alpha(z=0)}{Y_\alpha(z=\infty) - Y_\alpha(z=0)} = 0.9. \tag{12}$$

Its value can be obtained by the following equation, derived by Beigie *et al.* [3]:

$$\delta_{0.9}(t) = \sqrt{(4Dt)}\frac{\sqrt{(\overline{SR^2})}}{SR}. \tag{13}$$

The root mean square of the stretch ratio $\sqrt{(\overline{SR^2})}$ is obtained taking into account that the time average is performed on a time range from initial time t_o considered zero to a variable one t.

It has to be stressed that the mixing layer thickness $\delta_{0.9}$ is equal to $\sqrt{(4Dt)}$ when $SR(t) = 1$. This means that the mixing-layer thickness is equal to that obtained in not-stretched conditions. Furthermore, the factor $\sqrt{(\overline{SR^2})}/SR$ is always lower than 1 when the stretch ratio is greater than 1, as occurs in the mixing process, at least on average.

The analysis of the mixing layer, presented by means of the previous equations, is valid only when the distance from the origin of the coordinate to the nearest neighbouring intermaterial surface, in the direction of z, is much larger than $\delta_{0.9}$. In this case the boundary conditions of equations (8) and (10) can be considered constant in time and known.

To consider the mixing layers as an isolated transient 1-D diffusion process is a clear simplifications of the analysis of the whole process, so that in the experimental analysis it is important to compare the mixing-layer thickness with some characteristic lengths which are representative of the layers' interference. For such purpose some authors [3] have

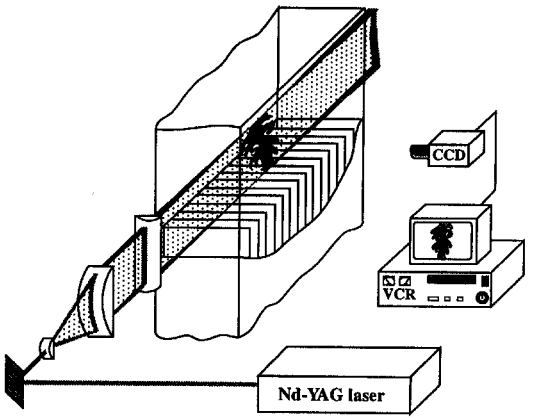

Fig. 1. Sketch of the experimental set-up.

defined the distance between the neighbour diffusion zones. More specifically this is the distance Δn of a point on the intermaterial surface from the nearest point on the interface along the direction normal to the interface. This distance will be termed the 'interface separation' and its relevance to the analysis of the mixing-layer interference will be discussed in the section devoted to the experimental results.

3. MEASUREMENT METHODOLOGY AND EXPERIMENTAL DEVICES

In order to face the difficulty mentioned in the introduction, the first requirement of the experimental flow to be investigated was fulfilled by choosing a flow which is 2-D or quasi-2-D. The generation of such flow was selected according to some general considerations about the turbulence level control and repeatability of inlet conditions. These considerations were discussed elsewhere [12, 13]. It turned out that a suitable set-up yielding such a fluid-dynamic pattern has to be constituted from a series of adjacent rectangular flows. The main characteristics of this set-up are depicted in the sketch in Fig. 1.

The test section of the experiment is a rectangular channel, which has been built with Plexiglas in order to have optical accessibility on all the four sides. In the first part of this channel, 32 adjacent rectangular ducts (5×100 mm cross-section) are mounted.

In order to analyse the mixing characteristics, interfaces and intermaterial surfaces two flows have been generated by means of some devices described later. In both types of surfaces (interface and intermaterial surfaces) the diagnostics problem is the same. It consists of detecting the concentration of some tracers, which in the present cases are either clouds of solid particles (TiO_2) or submicron particles produced by condensation and/or pyrolysis of gaseous material. The optical characterisation of the intermaterial surfaces was performed by recording the pattern of the light elastically scattered when the particulate is illuminated by a laser sheet. An Nd:YAG pulsed laser was tuned on the second harmonic wavelength ($\lambda = 532$ nm) and its beam was shaped by a set of cylindrical lenses in a sheet which was kept constant in thickness (500 μm) in all the experimental runs and was varied in height according to the extension of the objective field. The elastic scattered light was detected with a CCD camera equipped with a variable-focus telescope. The camera signal was recorded on a magnetic videotape and on a large memory computer after A–D conversion.

The generation of the interface is obtained by seeding the flow in one channel with submicron TiO_2 particles (0.2 μm). The TiO_2 particles have been dispersed in the air flow by means of a nubuliser which atomises a slurry of isopropyl alcohol and TiO_2. The particles reach the jet outlet after a long residence time, so that the alcohol is vaporised in the air. The interface corresponds to the discontinuity in the 2-D laser light scattering intensity due to the discontinuity of the tracer concentration.

The generation of an intermaterial surface between gaseous jets is more difficult because it has to be obtained only on a small fraction of the interface, and it has to be detectable for a long time interval. In principle, there are only two possibilities for generating an intermaterial surface with those characteristics. The first one is to tag for a short time a fraction of one of the two jets which has been previously seeded. This can be done, for instance, by using a phosphorescent seeding excited by a pulsed laser. This choice is not particularly convenient because the laser crosses the seeded volume inside a surface which is only in part an intermaterial surface. Therefore, it is difficult to discriminate between this last one and the whole contour of the seeded volume. The second choice is to produce a local seeding along a short segment of the interface near the outlet of the jet which shall be mixed. This has been performed in this work with a device which is based on a pulsed smoke wire technique.

The concept of such a device is shown schematically in Fig. 2. A thin layer of liquid is placed on a thin wire (Fig. 2a); the liquid is vaporised and/or partially pyrolised by electrical heating of the wire for a short

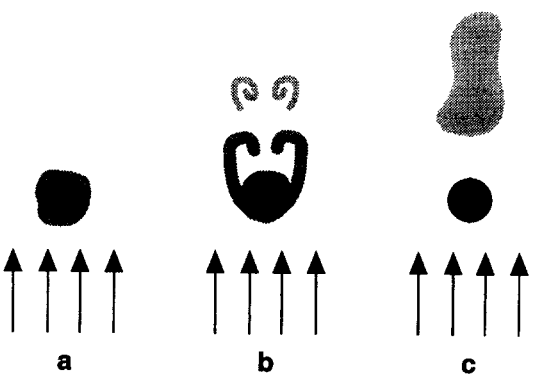

Fig. 2. Sketch of the operation of the pulsed smoke wire.

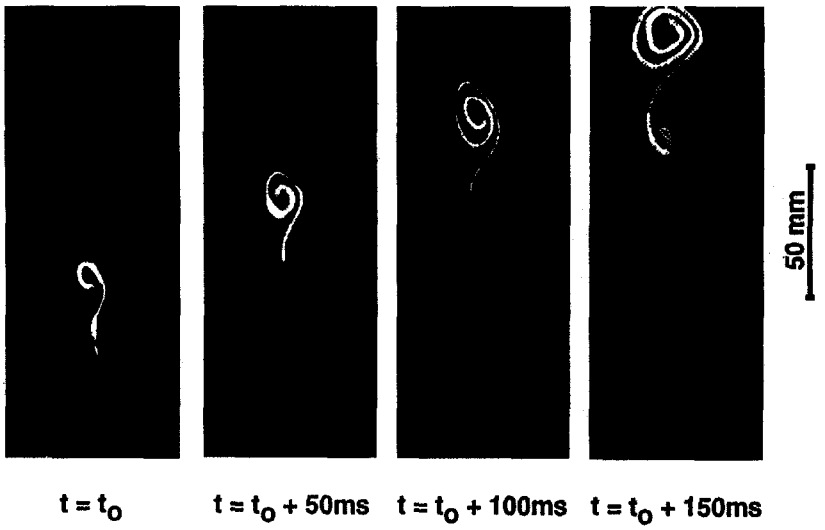

Fig. 3. Example of temporal evolution of intermaterial line.

time (Fig. 2b). Eventually the vapour or the pyrolysed product is condensed in a dense fog with a characteristic length comparable to the wire dimensions (Fig. 2c).

The energy transfer to the liquid is proportional to the electrical energy generated in the wire, that is:

$$E_w = \frac{V_w^2}{R_w}\Delta t_w = \frac{V_w^2}{\rho_w l_w} A_w \Delta t_w, \qquad (14)$$

where V_w, R_w, ρ_w, l_w, A_w and Δt_w are the voltage difference supplied to the wire, the resistance, the resistivity, the length, the cross-section of the wire and the electric pulse width (that is the time interval in which the voltage difference is supplied), respectively.

The resistivity ρ_w is determined by the chosen wire material (high temperature rupture resistance); in the present work Ni–Cr material has been used. The length is fixed by the constraint which requires the generation of a 'smoke' plume along the wider side of the jet cross-section (100 mm). The wire cross-section area has been chosen as small as possible to keep the thermal inertia as small as possible. But wires with diameters smaller than 100 μm were subject to frequent rupture. A good compromise was a 127 μm (0.005″) wire that has been used for all the tests reported. The pulse width ranged between 10 and 20 ms so that, according to the average velocity of the flow lapping the wire, a suitable intermaterial surface length could be generated. The voltage difference on the wire terminals could be varied up to 40 V.

Several liquids (silicon oil, water, α-methylnaphthalene, diesel oil) with different self-ignition characteristics and boiling temperatures have been tested. The most suitable liquid for producing a dense fog was tetradecane, which has been used in the measurement reported in this work.

An exemplifying sequence (20 Hz) of intermaterial surface, which is represented by an intermaterial line in this 2-D condition, is reported in Fig. 3. The pulse time and voltage are in this case 10 ms and 28 V. The jet on the right side of the lines was fed with an average velocity of 0.5 m s^{-1}, whereas the average velocity of the external air was 0.15 m s^{-1}. It is clear from the picture that the intermaterial line undergoes stretching and folding, so that a spiral structure with an increasing number of convolutions in time is formed. The stretch ratio between the intermaterial line extension at any time and that one detected as near as possible to the jet outlet has been evaluated. The extension of each intermaterial line has been measured on a hard copy reproduction of the detected image by means of a curvimeter with an error less than 5%, which resulted in a possible error on the stretch ratio of less than 10%.

4. RESULTS

The results, presented in this section, have been obtained under experimental conditions, which have been chosen with the purpose of obtaining the most effective roll-up of the interface under the constraint of keeping two-dimensionality. This was obtained by adjusting the exit average velocity of one flow at the highest level which was compatible with a reasonable extension of two-dimensionality. This was achieved by adjusting the average velocity at the exit of each rectangular channel to 0.2 m s^{-1}, apart from one of them (adjacent to the median plane) adjusted to 0.7 m s^{-1}.

4.1. *Interface*

Even though the main object of the paper is focused on methodological aspects in the experimental analysis of intermaterial surface, a preliminary short description of the flow in terms of the interface will be of some help in the interpretation of the results.

Figure 4 shows the visualization obtained by means

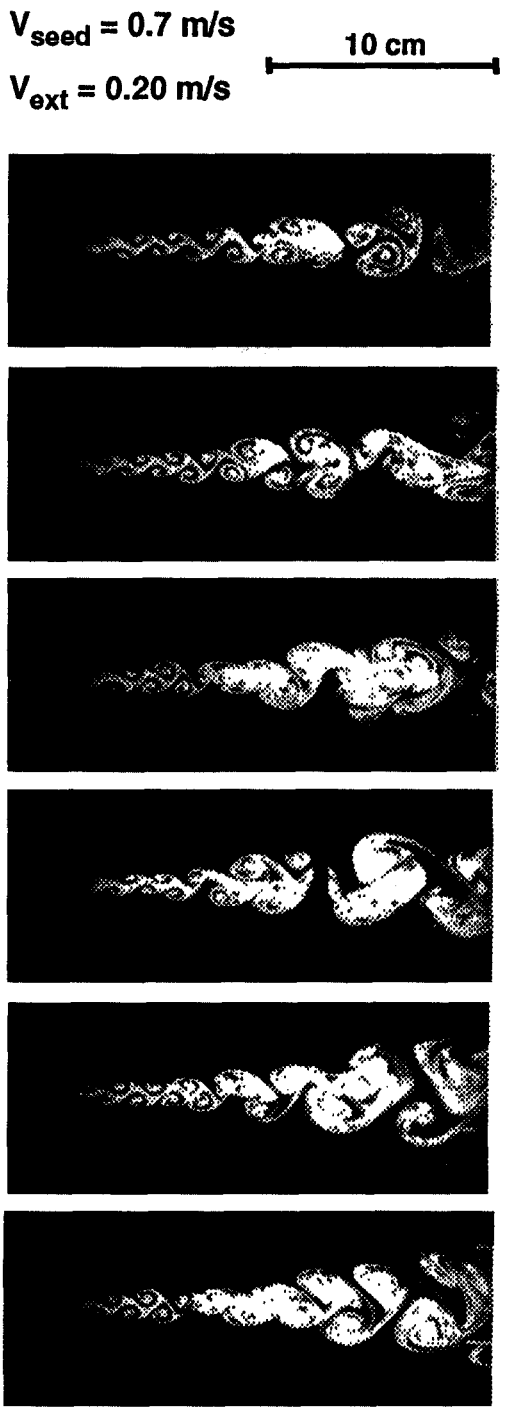

Fig. 4. 2-D LLS patterns of the seeded jet.

of the laser sheet technique, which has been previously described, for detecting the interface. The sequence of consecutive visualizations is taken at a 10 Hz frequency. The patterns show a very early (but weak) formation of oscillations of the whole jet and of antisymmetric vortices (the first two are clearly distinguishable). Later on, the number of convolutions in each single spiral structure increases and some couples of these structures are more in phase in the sense that they are more symmetric than before. It is not possible to determine whether these couples are formed according to the usual pairing process, as it has been described many times [14, 15], with the 'vortices' with the same sign (same angular rotation), since there is uncertainty whether they are relative to spirals of the same or opposite convolution. Each of this couple, that we call 'macro-structure', seem to shorten the distance from each other (not necessarily adjacent) and seem to pair by squeezing away one or a couple of spirals. Very large couples of spirals appear to be isolated with respect to the others, even though they are linked to the main spirals by extended filament-like structures.

A sharp discontinuity of TiO_2 particle concentration is detectable in the first part of the pattern. In the region far from the channel outlet, the discontinuity is not clearly observable due to the lack of adequate space resolution. Therefore higher magnification should be used when the intermaterial surface has to be detected with the purpose of measuring its extension. This consideration will be exploited when intermaterial surface results will be presented.

The interface characterisation has been exploited in previous works [12, 13] also to evaluate the extension in which the flow could be considered 2-D. This assessment was also performed by means of the comparison between the interface patterns, as those reported in Fig. 4, and the streaklines obtained by means of Lagrangian tracking of a suitable number of discrete particles introduced in a 2-D numerical simulation of the flow [12]. The degree of similarity between the experimental and numerical characterization was very high under a wide range of flow conditions, for an extension comparable to the object field used in the patterns detection of Fig. 4. Only in the final part of the patterns were some dissimilarities observed. These can be attributed to some 3-D effects, present in the experimental characterization, which could not be simulated by a 2-D numerical model.

Another evidence of the two-dimensionality was obtained [14] by means of the detection of the interface in cross-sections of the flow at different distances from the flow outlet. In this case the interfaces were constituted of parallel straight segments for 3/4 of the patterns reported in Fig. 4 and were slightly deformed in nearly parallel lines for longer distances. Therefore the final part of the patterns was considered quasi-2-D.

4.2. *Intermaterial surface*

The analysis of Fig. 4 showed that intermaterial surfaces cannot be detected with the same magnification ratio used for the detection of patterns reported in this figure. In fact the space resolution was not adequate to resolve the interface in the final part of the pictures and consequently intermaterial surfaces crossing those regions could not be resolved. Fur-

thermore, the use of only one camera in the detection of a sequence of intermaterial surfaces may entail an inadequate space resolution in detection of the first and last intermaterial surfaces. Here it is anticipated that finite stretch ratios were measured up to values of 70. The minimum resolvable length with the magnification ratio used in Fig. 3 was approximately 10 mm; therefore the last intermaterial line should be in the order of 700 mm. This means that the finite stretch ratios are integrated on too long a line, if some conclusions concerning local characteristics of stretching have to be drawn.

Finally, very high positive stretch ratios along the intermaterial line yield high negative stretch in the direction of the smoke thickness which can be smaller than the minimum objective pixel. Consequently, the laser light scattering from the smoke became too faint and it cannot be detected. In order to face these problems, one has to detect intermaterial surfaces in different adjacent objective fields, so that couples of consecutive intermaterial surfaces are comparable in extension and can be detected with the same suitable magnification ratios. Furthermore, the extension of the intermaterial line can be selected by adjusting the pulse time duration of the supplied voltage to the wire.

The time delay of the detection of the first intermaterial line is obtained by synchronising the video-signal, the wire pulse and the laser pulse, while the second material line is recorded after 0.05 s since the laser frequency is 20 Hz. For each couple of intermaterial lines 100 records have been performed and the finite stretch ratio has been evaluated. The distribution probability density function of these ratios have been computed. Some of these distributions are reported in Fig. 5. The symbol $\widetilde{SR}(t)\,|_{t_0}$ on the abscissae of these plots refers to the finite stretch ratios calculated between t and t_0. The first example in the highest part of the figure shows the probability density function (pdf) of the stretch ratios measured for couples of material lines which have been detected at 0.05 and 0.1 s after the smoke wire pulse. The stretch ratios range between 1.2 and 2.8, with a modal value around 2.2, and an average of 2.1. This is a peculiar case among the examples reported in the figure because this pdf presents a bell-shape type distribution, whereas all the other ones, relative to detection at longer times, show more asymmetric distributions. In fact both the modal and average values decrease with increase of detection time up to 0.25 s whereas the stretch ratio domain is limited by the smallest possible value (i.e. 1). Therefore the most probable events, far from the inlet region, occur in relatively unstretched conditions and only one side of the distribution is populated by events with high stretch. It is also of interest to underline that the average values for detection times higher than 0.25 s are relatively constant and they range between 1.35 and 1.45. This aspect is also shown in Fig. 6, in which the ensemble averages of the stretch rates $\bar{\tilde{K}}$ obtained according to

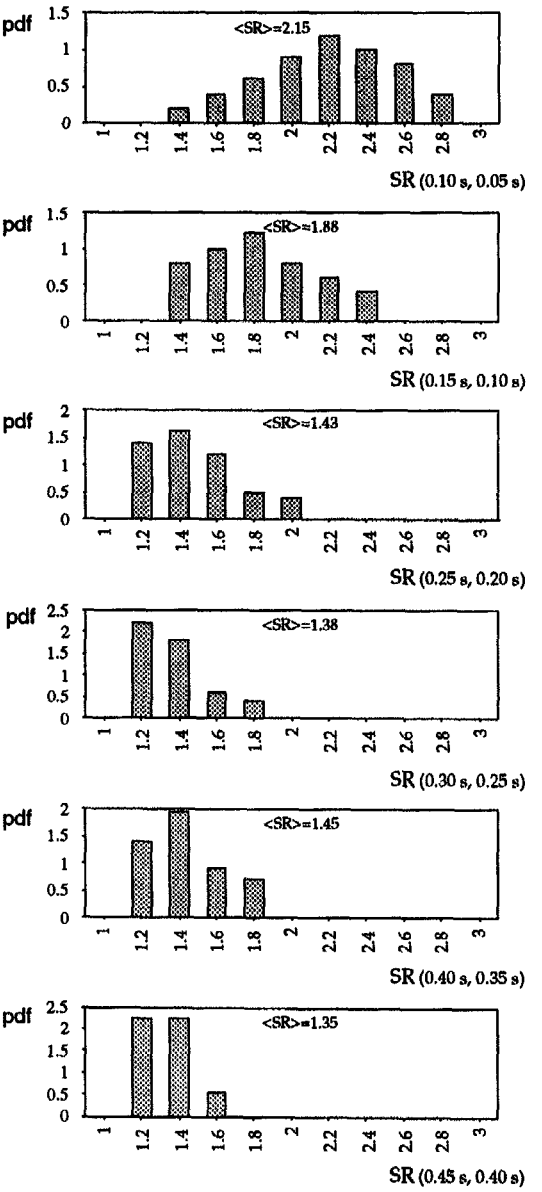

Fig. 5. Probability density function of the stretch ratio $\widetilde{SR}(t)\,|_{t_0=t-0.05}$.

equation (7), are plotted vs the detection time. In fact the behaviour of the plot is characterised by two different trends for times shorter and longer than 0.2 s. In the first one, the stretch rate decreases with a nearly constant slope, whereas in the second one it is nearly constant around 6 s^{-1}.

In the same plot, the finite stretch ratio $\widetilde{SR}$ between the initial time, in which the smoke pulse is ended, and the detection time of a second material line is reported. This quantity cannot be measured with only one magnification ratio, as has been discussed before, so it has been obtained as the product of a sequence of the stretch ratio averages which could be measured

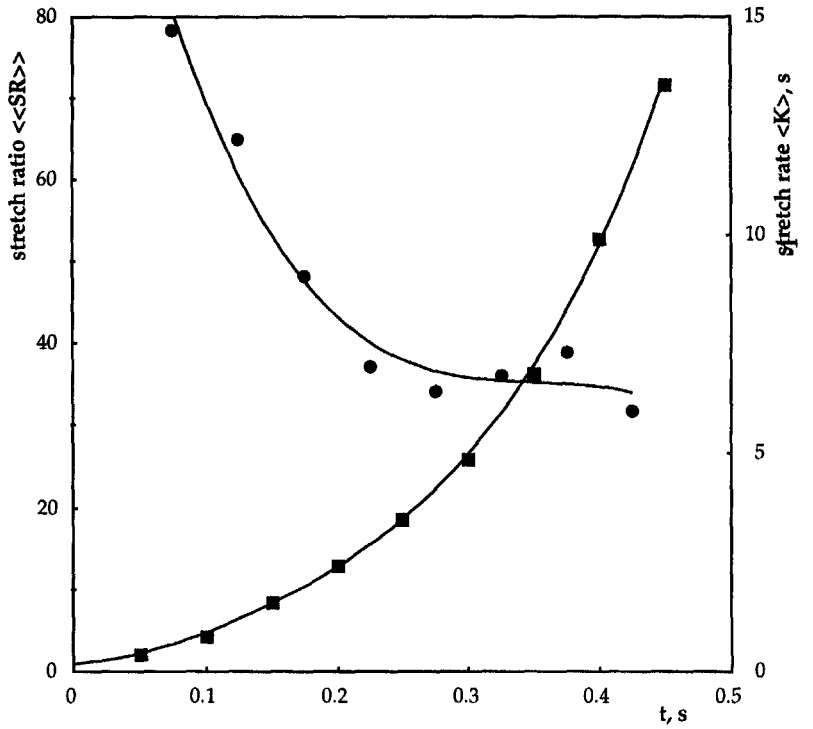

Fig. 6. Variations of ensemble average of finite stretch rate (●) and finite stretch ratio (■) with the detection time.

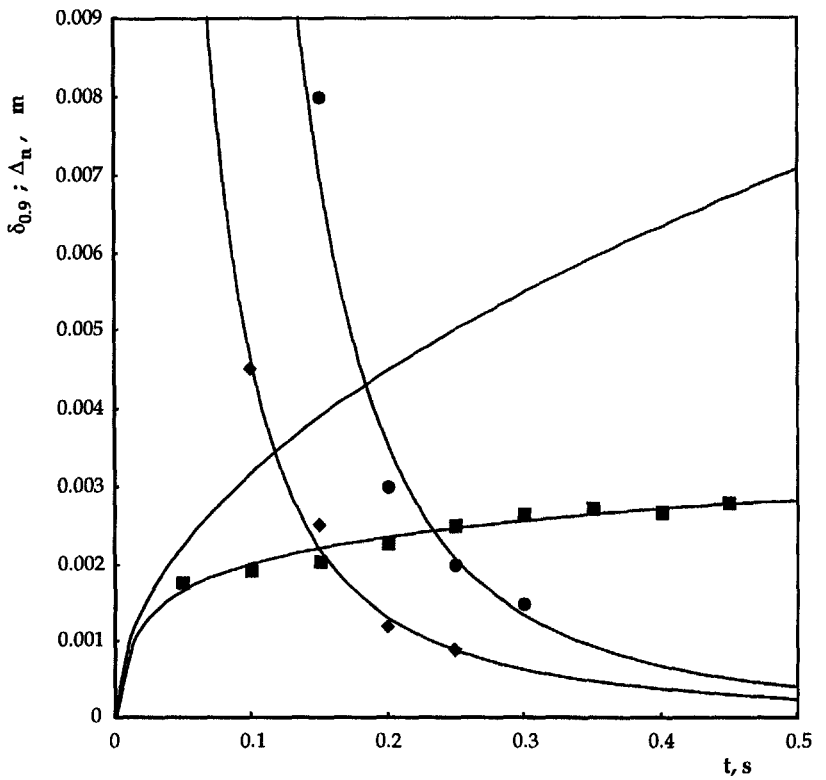

Fig. 7. The time variation of unstretched mixing-layer (——), stretched mixing-layer (■), interface separation distance (● average, ◆ minimum).

on couples of consecutive intermaterial lines detected once at a time with suitable magnification ratios. In other terms it is given by the following formula:

$$\langle\langle \widetilde{SR}(t)|_{t_0=0}\rangle\rangle = \langle \widetilde{SR}(0.05)|_{t_0=0}\rangle \langle \widetilde{SR}(0.1)|_{t_0=0.05}\rangle \ldots \langle \widetilde{SR}(t)|_{t_0=t-0.05}\rangle. \quad (16)$$

The ensemble average on the left side of the equation should not be interpreted as a true ensemble average. In fact, the product on the right side is only an approximation of the ensemble average of the finite stretch ratio $\langle \widetilde{SR}\rangle$. The approximation has been evaluated to be less than 10% in the sense that both types of averaging, $\langle\langle \widetilde{SR}(t)|_{t_0=0}\rangle\rangle$ and $\langle \widetilde{SR}(t)|_{t_0=0}\rangle$, are available for sequences formed by three consecutive detections of material lines and the difference between the two is less than 10% of the $\langle \widetilde{SR}\rangle$ values. A second approximation has also been used in the evaluation of $\langle\langle \widetilde{SR}(t)|_{t_0=0}\rangle\rangle$ reported in Fig. 6 since the first term of the product $\langle \widetilde{SR}(0.05)|_{t_0=0}\rangle$ at 0.05 s is an estimation of the real value. In fact, from some preliminary experiments, it was known that the condensation time for the formation of the smoke line was around 0.02 s so that the measurements of the stretch in that time range are overestimated with respect to the real one, because the increase of the smoke line has also to be attributed to particulate formation. The choice was made of attributing to the stretch ratio at 0.05 s, the same value measured at 0.1 s. This has to be considered as an underestimation with respect to the value obtained by considering the real stretch ratio occurring between 0 and 0.05 s since it is expected that the maximum stretch occurs very early in the flow interaction. Consequently the whole profile of the product of the terms $\langle\langle \widetilde{SR}(t)|_{t_0=0}\rangle\rangle$ is affected by a factor, which, at present, cannot be measured, but should be higher than 1. In any case the trend of the stretch ratio profile in Fig. 6 presents a clear characteristic which is not affected by this indetermination. It increases in the whole temporal range in which the measurements have been performed and it reaches a maximum value which is at least 70.

According to the analysis presented in Section 2, the stretch ratio is relevant to determine the mixing-layer thickness. In fact, when the intermaterial surface undergoes significant stretch the maximum layer thickness can be evaluated by using the values of the finite stretch ratio of Fig. 6 in equation (13). The mixing-layer thicknesses evaluated in such a way are plotted in Fig. 7 with square symbols. In order to stress the differences, the thickness obtained in unstretched conditions, assuming a stretch rate equal to 1 (that is $\delta_{0.9} = \sqrt{(4Dt)}$), is also plotted in the same figure with a continuous line. In both cases $\delta_{0.9}$ increases with time, but it is clear that the difference between the two thicknesses also increases because of the stretch presence.

A second set of measurements has been performed on the same images exploited for the evaluation of the stretch ratios. These are relative to the interface separation (Δn) defined in Section 2. The measure is obtained by considering the median point along each detected material line and by measuring the distance between this point and the nearest point of the intermaterial line along the normal to the surface. In Fig. 8 the probability density function of the interface distance measured at different times is reported. Also in this case the measurements could be performed only for times longer than 0.05 s because of the aforementioned problems related to smoke line formation. This fact is not important because the interface detected in the early part of the flow interaction was always nearly straight so that interface separations could be considered infinite at 0.05 s. In fact, if the interface in this early region is nearly straight (as it is shown in the left side of the pictures reported in Fig. 4), the intermaterial surfaces are not convoluted because they are a fraction of the interfaces at different times.

This characteristic is partially kept at $t = 0.1$ s. In fact the pdf at this time, reported in the higher part of Fig. 8, shows that a great percentage of the events are relative to infinite interface separation. The other events are relative to Δn which range between 3.5 and 6.5 mm with a pronounced modal value at 5 mm. Therefore the pdf appears to be bimodal with an ensemble average $\langle \Delta n\rangle$ at 8.1 mm. At the following detection time ($t = 0.15$ s) all Δn are finite. They are more probable around the modal value at 3 mm even though they are distributed in a larger range of values up to 10 mm. At times 0.2, 0.25 and 0.3 s, the events are always distributed around their ensemble averages, which are not significantly different from the modal values and which decrease continuously with time. This last point is also illustrated by the profile of the ensemble average vs the detection time, plotted in Fig. 7 with round symbols. The trend of the interpolating line shows that a significant decrease occurs in the time interval between 0.1 and 0.15 s. In the same figure the minimum values of the interface separations are also reported with rhomb symbols. The trend of the interpolating curve is similar to that relative to the average estimation, the events corresponding to the minimum value occur around 0.05 s earlier than those relative to the average ones. The importance of the comparison between the mixing-layer thickness and the interface separation will be presented in the following section.

In the discussion of the results the average position of the intermaterial lines will be also of interest. Therefore this type of measurements has been performed on the same ensemble of images used for the previous measurements. The median point along the curvilinear segment has been determined and its distance from the outlet has been computed by means of simple computer program. The averages of these distances reported in Fig. 9 are interpolated against time with constant slope up to 20 mm, which in corresponds to a constant velocity of 0.7 m s^{-1}. Later on the slope

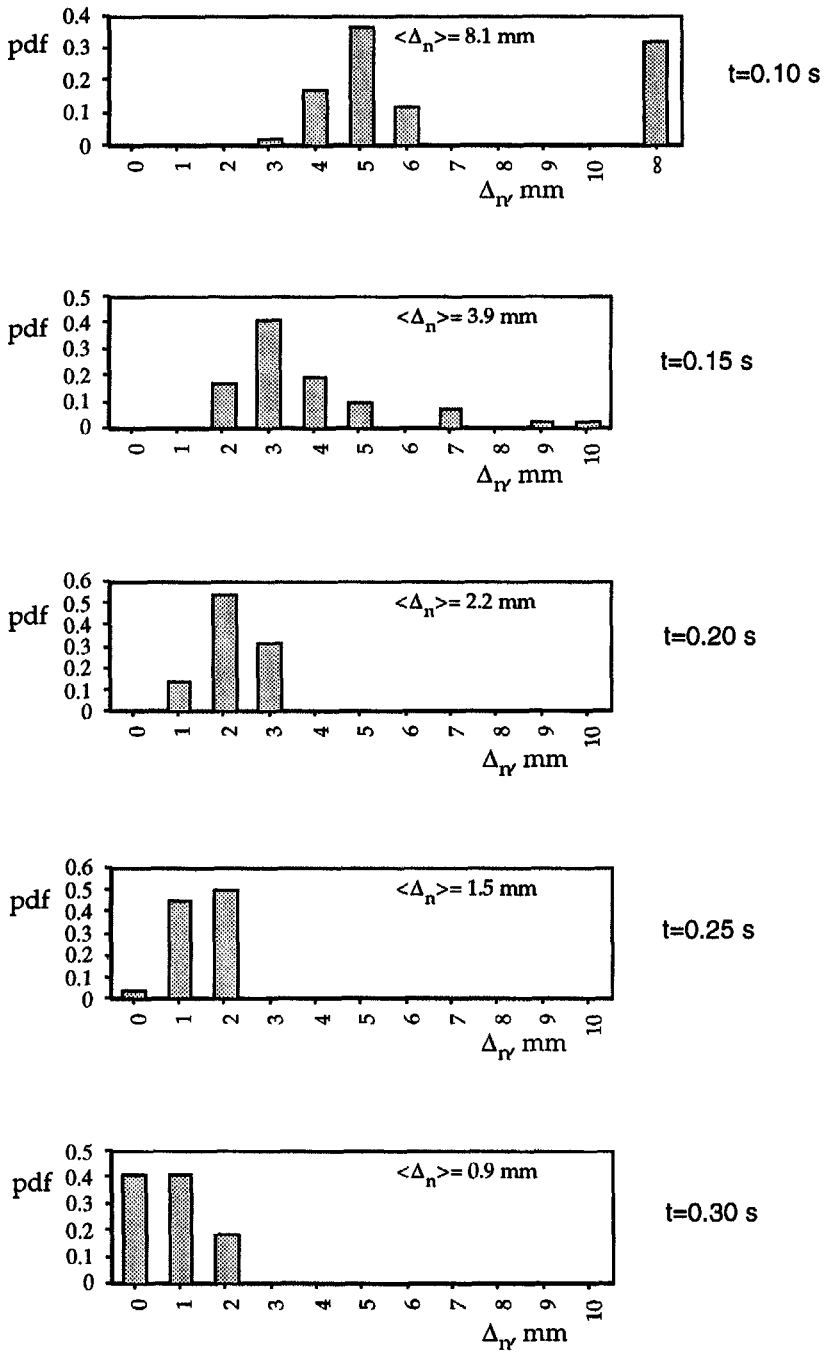

Fig. 8. Probability density function of the interface separation distance at different detection times.

continuously decreases, since the velocity of the material line is more controlled by the external flow. The standard deviation is quite low ($\sigma < 0.1$) so that in this particular flow the location of the intermaterial surface at a fixed time can be reasonably assessed.

5. DISCUSSION

5.1. *Diagnostics aspects*

The experimental method for generating intermaterial surfaces, presented in this paper, seems to be a unique choice in the case of gaseous systems. In fact an intermaterial surface is formed by a tracer which, by definition, is a non-diffusing, fully-convected material. This means that no gaseous components can be used for such a purpose because it is not possible to prevent their diffusion. However, the diffusion of particles dispersed in a gaseous medium can be considered negligible with respect to gaseous diffusion. In this case particles have to be dragged in such a way that they are representative of the gas

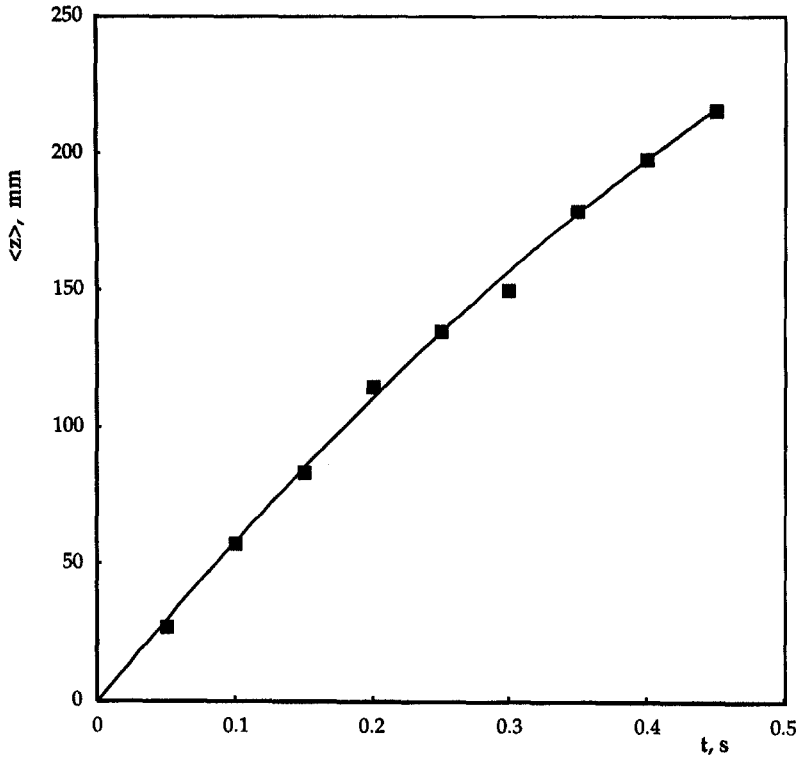

Fig. 9. Streamwise distance of intermaterial line centre from the jet outlet.

displacement. These two requirements (low particle diffusivity and high particle drag) are generally evaluated in terms of Schmidt and Stokes numbers. The Schmidt number is defined as the ratio between momentum (kinematic viscosity) and mass diffusivity coefficient ($Sc = \nu/D$). It is approximately 1 when ν_{gas} and D_{gas} refer to gas media, whereas it is much higher than 1 with particles, and it is in the order of 10^6 for particles of 1 μm diameter [16]. The Stokes number [17] is defined as $St = \rho_p d_p^2/18\mu_g\tau_g$, where ρ_p and d_p are density and equivalent diameter of the particles, μ_g is the dynamic viscosity of the gas, τ_g is the aerodynamic time-scale with respect to particle response time evaluation. This can be evaluated as the ratio $\tau_a = \delta/\Delta v$, where δ and Δv are the characteristic length-scale and velocity across the mixing-layer. According to the results of Fig. 7, δ is in the order of 1 mm and Δv, from a conservative evaluation, is the difference of the average velocities of the jets (0.7−0.2) m $s^{-1} = 0.5\,m\,s^{-1}$. Therefore the aerodynamic time-scale is in the order of 2×10^{-3} s, so that the Stokes numbers are smaller than those obtained for submicron particles dispersed in a gaseous medium. For instance, for the TiO_2 particles, used for the interface characterization, the Stokes number is smaller than 10^{-3} taking into account that the largest particle size is 0.3 μm and the apparent density is 0.95 kg dm^{-3}. In the case of the smoke particulate formed by condensation of vaporised–pyrolysed gaseous products, the Stokes number should be in the order of 10^{-2}, since the particle size is around 1 μm [18]. Apart from these considerations, concerning the technical capability of producing submicron particles, it is worthwhile to stress again that this type of particulate, for which $Sc_p \gg 1$ and $St \ll 1$, is the only possible choice of tracer in a gaseous system.

A second unique feature of these techniques, employed for the intermaterial surface characterisation, is that the tracer has to be released or tagged impulsively, so that only a small part of the interface is characterised. The drawbacks relative to tagging a pre-existing tracer have been discussed in the section devoted to the experiments, whereas those linked to the pulsed release of a tracer deserve some other comments. The injection of material in a fluid-dynamic field is generally intrusive and perturbative. In the case of intermaterial surface generation the intrusivity can be considered negligible because the injection has to be performed on the border of the jet confinements. In particular for the smoke-wire device, described in this paper, it is not important because the wire was smaller than the plate thickness on which it was placed and it can be considered part of the confinements. Some perturbations can be introduced in the field due to heat and mass release. In the present case these effects were limited because the electric power was adjusted in such a way that the energy was deposited only on a liquid phase. An experimental check to ensure a low level of perturbation was performed by detecting the interface both in the presence and in the absence of the electric pulse. Only for pulse voltages higher than 35 V and longer than 15 ms, the interface

changes its shape from a linear straight contour to an irregular one.

The final comment, devoted to the diagnostic aspects, concerns the difficulty of performing Lagrangian measurements in a wide control volume. The causes of these difficulties have been discussed in the introduction. In synthesis, they relate to the need to cover the control volume with a large number of contiguous detectors, which are not available with the present technology. Therefore, in this work it was decided to keep the whole spatial domain of measurement as small as possible. This resulted in a characterization of a 2-D field which could be ensured for the first 150 mm of the seeded jet extension, which correspond to 0.3 ms residence time of a material point on the interface.

Even though the methodological aspects of the mixing analysis can be fully discussed in this temporal range, the measurements were extended in a longer temporal range, because, at least in their statistical average, they are representative of the stretch. For instance, it is interesting to note that, with the 2-D loss, the stretch rate reported in Fig. 6 is nearly constant for times longer than 0.3 ms, so that it will be important to verify in the future whether this is a general characteristic of the transition from 2-D to 3-D flows. The constraint of the finiteness of the detector number necessitates performing statistical analysis of couples of consecutive intermaterial lines, whereas it would be important to perform measurements of the stretch ratios between couples of intermaterial lines detected after a long period from each other. In fact the stretch ratios, reported in Fig. 6, are not obtained as direct ensemble averages of the measurements, but as the product of partial averages of consecutive intermaterial lines according to equation (16). Even though devices with a very large number of contiguous detector elements will be available in the future, this constraint seems to be the most restrictive one in any Lagrangian measurement which is not limited to the aim of only following the trajectory of a single point with its related properties (e.g. mass concentration, temperature).

Other technical features of the diagnostics used in this work are not dealt with here because they are less important from a methodological point of view, on which we are focused at present. However, the analysis of the mixing process deserves a deep discussion in order to emphasize the generalization of the analysis derived from the measurements presented in this paper.

5.2. *Mixing analysis*

A synthesis of the whole set of the results is given by the plots in Fig. 7. The square and round symbols represent, respectively, the average values of the mixing-layer thickness and the separation distance of the interface. The two interpolating curves, fitting the experimental data, cross approximately at $t^* = 0.23$ s. This time t^* can be chosen as an upper limit of a temporal domain in which the mixing layers can be considered isolated. Of course this is a criterion which is arbitrary because it is based on an average value. A more restrictive criterion is to choose the time at which the smallest separation distance (rhombs) is equal to the largest possible mixing-layer thickness (continuous line), which is of course that one evaluated in non-stretched conditions. In both cases, one is capable of identifying a peculiar mixing regime, which we call the '*isolated mixing-layer regime*', where the mixing analysis is simplified both in terms of physical understanding and of numerical modelling. In fact, in this case, the hypothesis of a 1-D time-dependent diffusion process can be exploited in a convenient way, because the whole mixing-layer can be described in terms of equations (8) and (10) under well-defined boundary conditions. In fact the mass fraction for $z \to -\infty$ and $z \to +\infty$ are given by the inflow conditions ($Y_{-\infty}, Y_{\infty}$). It is worthwhile to stress that in this regime ($t < t^*$), the probability density function of the interface separations (as reported in Fig. 8) is not important in respect to the mixing process, because the distances of neighbouring segments of the interface are larger than the mixing-layer thickness, which is the only relevant length-scale. However, this probability density function is important in evaluating the following part ($t > t^*$) of the process, as is shown by comparing Figs. 5 and 8. In fact, the probability density function of the stretch ratios (Fig. 5) and of the interface separation (Fig. 8) shows some similar features. In both cases with time they become less disperse and their ensemble average decreases. This means that it is possible that they reach a regime in which the stretch is negligible, and the separation distance distribution does not change with time. This situation is comparable to the pseudo-turbulent conditions discussed by Gibson [19], who named this peculiar condition fossil turbulent. In this case the convective stirring is negligible and the evolution of mass fraction distribution is simply described by non-stretched diffusive mixing. In the other case, in which the stretch is still active after the characteristic time t^*, the analysis becomes more complex, but the knowledge of the joint probability function of stretch ratios and the interface separation is, in principle, the controlling parameter on which models based on the explicit formulation of mass fraction spatial structure are developed [1, 3, 17]. The measurement of this joint probability function is a challenging task, because of the mentioned difficulty of direct averaged measurements of the stretch ratio $\widetilde{SR}(t)|_{t_0}$ at a large detection time t, but it will be a crucial step in the future development of the experimental analysis of turbulent mixing in terms of the methodology presented in this paper.

The final comment is devoted to the importance of the feasibility of measuring the stretch rate in the early part of the gaseous mixing-layers in the presence of reactions which evolve in time-scales much smaller than the diffusion time. This is the case of turbulent diffusion flame, for which extensive analysis has been

performed in terms of the stretch rate [7, 8] or of some equivalent quantity like the dissipation rate [5, 6]. In this case the stretch rate significantly affects the chemical kinetics and the possible heat release related to it. In particular, it is well known that diffusion flames are stabilised only if the stretch rate is lower than critical values evaluated in steady or non-steady conditions. The technique, used in this work, is useful in such kinds of analysis, because, as has been stressed before, it is particularly suitable in the analysis of the near field of the mixing process.

6. CONCLUSIONS

An experimental method for the analysis of the gaseous mixing process in terms of Lagrangian quantities has been described and used for the characterisation of a prototypical fluid-dynamic configuration. The analysis has allowed the identification of the merits and the limits of the method. The main advantage of the technique consists of the complete characterisation of the mixing process in a space–time domain which can be experimentally identified by comparing the mixing-layer thickness with the separation distance between neighbouring segments of interfaces. When the layer is smaller than the interface separation, a regime, named the 'isolated mixing-layer regime', is identified. In this case the experimental characterisation of a measurable Lagrangian quantity (the stretch ratio) is sufficient to describe the whole isothermal mixing-layer. The same quantity expressed in terms of its derivative (stretch rate) is also sufficient to describe reactive mixing-layers. The main limit of the experimental method relates to technological constraints rather than to its principles. In fact, it is due to the finiteness of the number of contiguous detectors available at present. This constraint entails that an intermaterial surface can be detected with sufficient space resolution only in a 2-D domain and for a limited range of length-scales. Therefore, it seems difficult that the technique can be used directly in multi-dimensional flow like turbulent ones, but it will be very useful in the characterisation of prototypical flows, which can be considered as elementary spatial–temporal structures of more complex flows.

REFERENCES

1. J. M. Ottino, Description of mixing with diffusion and reaction in terms of the concept of material surfaces, *J. Fluid Mech.* **114**, 83 (1982).
2. J. M. Ottino, *The Kinematics of Mixing: Stretching, Chaos and Transport*. Cambridge University Press (1989).
3. D. Beigie, A. Leonard and S. Wiggins, A global study of enhanced stretching and diffusion in chaotic tangles, *Physics Fluids* **A3**(5), 1039 (1991).
4. C. H. H. Chang, W. J. A. Dahm and G. Tryggvason, Lagrangian model simulations of molecular mixing, including finite rate chemical reactions, in a temporally developing shear layers, *Physics Fluids* **A3**(5), 1300 (1991).
5. F. Mauss, D. Keller and N. Peters, A Lagrangian simulation of flamelet extinction and re-ignition in turbulent jet diffusion flames. In *Proceedings of the Twenty-Third International Symposium on Combustion*, The Combustion Institute, Pittsburgh, p. 693 (1991).
6. P. K. Yeung, S. S. Girimaji and S. B. Pope, Straining and scalar dissipation on material surfaces in turbulence: implications for flamelets, *Combust. Flame* **79**, 340 (1990).
7. A. F. Ghoniem, M. C. Soteriou, B. M. Cetegen and B. M. Knio, Effect of steady and periodic strain on unsteady flamelet combustion. In *Proceedings of the Twenty-Fourth International Symposium on Combustion*, The Combustion Institute, Pittsburgh, p. 233 (1992).
8. R. S. Barlow and J. Y. Chen, On transient flamelets and their relationship to turbulent methane–air jet flames. In *Proceedings of the Twenty-Fourth International Symposium on Combustion*, The Combustion Institute, Pittsburgh, p. 231 (1992).
9. J. M. Ottino, Mixing, chaotic advection and turbulence, *Ann. Rev. Fluid Mech.* **22**, 207 (1990).
10. R. Chella and J. M. Ottino, Conversion and selectivity modifications due to mixing in unpremixed reactors, *Chem. Engng Sci.* **39**, 551 (1984).
11. E. L. Cussler, *Multicomponent Diffusion*, Chemical Engineering Monographs 3. Elsevier Scientific Publishing Company, Amsterdam (1976).
12. A. Cavaliere, G. de Felice, F. M. Denaro and C. Meola, Eulerian and Lagrangian simulation of transport phenomena in multiple or periodical interacting planar jets and wakes versus experimental results. In *Proceedings of Computational Methods and Experimental Measurements*, p. 135. Springer-Verlag (1993).
13. A. Cavaliere, M. El-Naggar, R. Ragucci, G. Vanacore and C. Venitozzi, Transition flow regimes in a series of adjacent rectangular jets. In *Proceedings of Turbulence and Vorticity*. CUEN Press (in press).
14. M. S. Husein, J. E. Bridges and F. Hussain, Turbulence management in free shear flows by control of coherent structure. In *Transport Phenomena in Turbulent Flows*, p. 111. Hemisphere Publishing Corporation, NY (1988).
15. M. Lesieur, C. Staquet, P. LeRoy and P. Comte, The mixing layer and its coherence examined from the point of view of two dimensional turbulence, *J. Fluid Mech.* **192**, 511 (1988).
16. D. E. Rosner, *Transport Processes in Chemically Reacting Flow Systems*, p. 122. Butterworths, Boston (1986).
17. C. T. Crowe, J. N. Chung and T. R. Troutt, Particle mixing in free shear flows, *Prog. Energy Combust. Sci.* **14**, 171 (1988).
18. T. J. Mueller, *Handbook of Flow Visualization*, Chap. 5, p. 45. Hemisphere Publishing Corporation, NY (1989).
19. C. H. Gibson, Kolmogorov similarity hypotheses for scalar fields: sampling intermittent turbulent mixing in the ocean and galaxy. In *Proceedings of the Royal Society of London*, **A434**, p. 149 (1991).